ELECTROSPUN SCAFFOLDS WITH RHAMNOLIPIDS TO TREAT DEPLETED URANIUM CONTAMINATED WOUNDS

By Brenda Padilla

A Thesis

Submitted in Partial Fulfillment

of the Requirements for the Degree of

Master of Science

in Biology

Northern Arizona University

May 2023

Approved:

Robert S. Kellar, Ph.D., Chair

Adonna M. Rometo, Ph.D.

Aaron J. Tabor, Ph.D.

ABSTRACT

ELECTROSPUN SCAFFOLDS WITH RHAMNOLIPIDS TO TREAT DEPLETED URANIUM CONTAMINATED WOUNDS

BRENDA PADILLA

Depleted uranium (DU) is a metal by-product produced after the enrichment of natural uranium (U) to lower its radioactivity for military use. Although most radioactive isotopes have decayed, DU remains toxic and a radioactive health hazard when ingested or inhaled into the body. Currently, there are over 500 abandoned uranium mines located in the American Southwest that pose a threat to the surrounding environment and to the population's health through the ingestion of contaminated water. Previous publications from our lab demonstrate that exposure to DU has negative effects on the natural wound healing process through a variety of cytotoxic mechanisms; however, current literature lacks a healing therapeutic to counteract this issue. Therapeutics, such as novel wound coverings, have been developed to promote the wound-healing process by treating wounds with three-dimensional biomaterials made to mimic the extracellular matrix. These biomaterials are often applied to effectively promote cellular migration and proliferation. In the current study, we propose that these novel electrospun wound healing scaffolds can be impregnated with unique chemical agents to facilitate delivery into the wound bed in an effort to neutralize or de-contaminate the tissue from DU exposure. First, an *in vitro* wound model was prepared using human dermal neonatal fibroblasts (hDFn) in combination with rhamnolipids, a 'green' biosurfactant with known environmental contaminant binding properties. Using this *in vitro* wound model, cells exposed to DU and treated with rhamnolipids had an increased percent closure rate over cells only exposed to DU. These preliminary findings provide proof of concept for the continued exploration of using rhamnolipids as a treatment for DU-contaminated wounds. Subsequently, this work focused on incorporating rhamnolipids into novel electrospun wound healing scaffolds cellularized with fibroblast cells to assess biocompatibility utilizing the scanning electron microscope (SEM). Cytocompatibility assays were also conducted to measure the effects on hDFn cells' metabolism and viability when inoculated with rhamnolipids in growth media. These rhamnolipids are of particular interest due to their non-toxic nature, antimicrobial properties, and affinity to bind to metals of environmental concern, like uranium. This study is among the first to explore the effects of rhamnolipids as a treatment against internal DU exposure by using electrospun scaffolds as a healing therapeutic to treat those individuals affected by chronic exposure to U-contaminated water throughout the American Southwest.

ACKNOWLEDGEMENTS

I would like to thank my P.I., Dr. Robert Kellar for your guidance, generosity, and most of all, mentorship during these last two years. As well as my committee members Dr. Adonna Rometo and Dr. Aaron Tabor. I am forever grateful you all allowed me the opportunity to learn from each of you. Secondly, I would like to thank Dr. Catherine Propper and Dr. Anita Antoninka for their unwavering support throughout my time in the RISE program. You must know the impact you have on students remains long after graduation.

Por mi amá y apá, por todo su esfuerzo en ayudar me seguir para adelante durante mis seis años en la universidad. Ustedes me ensenaron lo que significa ser fuerte y madura en esta vida. Con su apoyo, este diploma es tanto mío como de ustedes. Los quiero muchísimo y si me puse las pilas. También dedico este trabajo a mi abuelita, te quiero un chingo. Y ah mi abuelito, que en paz descanse, te quiero.

A special thank you to Marge for sharing their endless knowledge with me inside and outside the lab. There is no one I'd rather watch anime with in between long experiments. Taylor, you know how special you are to me. You are an amazing lifelong friend, and I cannot wait to see where life takes you (I know you'll get far). This work is as much mine as it is yours. Oscar, you inspire me every day. Your love and support have pushed me farther than I thought possible. Thank you for being the best life partner in all the universe.

This work was supported by the Research Initiative for Scientific Enhancement (RISE, 1R25GM127199-01). Thank you to Ron Allen at the NAU Imaging and Histology Core Facility for help with SEM images, and Development Engineering Sciences, LLC for assistance with electrospinning.

TABLE OF CONTENTS

LIST OF FIGURES

CHAPTER 1

Introduction

1.1 Uranium background

Uranium (U) is a naturally occurring element consisting of three primary isotopes: U-234, U-235, and U-238 (EPA, 2023). All U isotopes behave alike chemically but differ radioactively (Keith *et al*., 2013). Natural uranium is used to create enriched uranium, which is radioactive and is required as fuel for nuclear power reactors (Keith *et al*., 2013). The resulting metal by-product following the enrichment process of natural U is known as depleted uranium (DU) and predominantly consists of U-238 (99.8% by mass) with trace amounts of U-235 (0.2% by mass) and U-234 (0.001% by mass) (IAEA, 2023). Depleted uranium is less radioactive than natural U and often used for military purposes (Keith *et al*., 2013). However, natural and depleted uranium exhibit the same chemical effects on the body (Shaki, 2019).

Throughout World War II, large-scale U-mining became a purposeful and concentrated war effort in response to an impending nuclear arms race (Briner, 2010). The United States (US) Atomic Energy Commission set to purchase uranium ore excavated within the US until the late 1960s, launching a surplus of mining throughout the American southwest, including Arizona, Colorado, New Mexico, and Utah (Brugge, 2002). Subsequently, there was a focus on decreasing the toxicity of uranium across battlefields.

Historically, DU was introduced into the military's initiative to incorporate the dense metal into tanks, and anti-armor ammunition due to its high density and penetration ability during the Persian Gulf War, the Balkans conflict, the Afghan War, and the second Persian Gulf War (Briner, 2010). Although most of the radioactive isotopes have decayed, DU remains toxic and a health hazard when ingested or inhaled into the body as DU emits alpha particle radiation

(Briner, 2010; EPA, 2023). Although alpha particle radiation does not have a sufficient amount of energy to pierce through the skin (EPA, 2023), the use of DU as an armor-piercing projectile can result in the release of U into the surrounding environment due to its pyrophoric nature and adiabatic shearing (IAEA, 2023). Upon impact, DU particles can also potentially aerosolize and enter the airway (IAEA, 2023). Elevated levels of U found in the environment are concerning due to the radioactivity and chemical toxicity exhibited and can lead to an increased risk of exposure for those living near where DU weapons are being used (Erikson, 1990; Keith *et al.*, 2013). In addition to the environmental contamination of the soil within warzones, military projectiles can chemically react with surface water, where U may then be oxidized and leached into groundwater and transported into water sources (Erikson, 1990).

1.2 Uranium and the Navajo Nation

Located on the U-mining belt, the Navajo Nation was pulled into the ongoing mining "boom" (Brugge, 2002). From the mid-1900s to the late 1980s, close to 30 million tons of uranium were excavated from the Navajo Nation alone (EPA, 2023). During this time, many Navajo men worked in the mines and raised their families within close proximity to the mining mills, without any indication of the threat U exposure may produce to nearby homes and water sources with elevated levels of radiation (Brugge, 2002; EPA, 2023). Although these mines are no longer in use, the repercussions of the mining "boom" brought onto the Navajo people by the U.S. remains, as upwards of 500 abandoned uranium mines still reside throughout the Navajo Nation (Hoover, 2017).

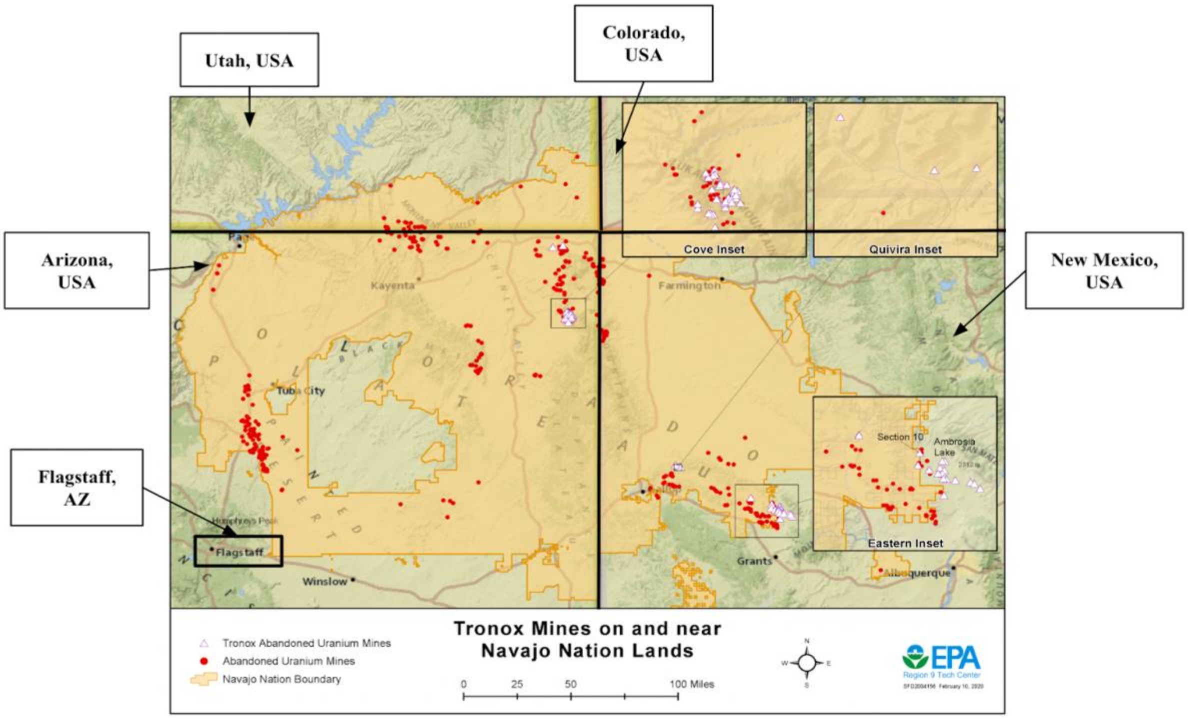

Figure 1. Map overview of the 523 abandoned mine sites across the Navajo Nation. Uranium leaching from these mine sites has resulted in elevated U levels found in water sources. Chronic exposure to uranium can lead to serious health effects, including kidney disease, and lung and bone cancer (EPA 2023).

The Navajo Nation is located in the American Southwest, where the majority of the population lives in rural communities and approximately 30% of households do not have access to proper water infrastructure (Hoover, 2017). The abandoned U-mines continuously present a threat to the Navajo community with unregulated water sources that are hardly tested for heavy metal contaminants or other known environmental toxins (Hoover, 2017). Subsequently, those living in underserved and rural communities may be uninformed of the potential health risks brought on by chemical exposure through chronic consumption of contaminated water (Backer and Tosta 2011; Shrivastava 2015).

Samples gathered from 464 of the unregulated water sources currently residing on Navajo land were tested for uranium. For reference, the EPA established the maximum contaminant level (MCL) for uranium at 30 µg/L (EPA, 2023). Approximately 12.5% of these water sources were found to have exceeded the MCL for uranium (Hoover, 2017). Possible health effects from internal uranium toxicity have been shown to increase the risk of lung cancer, kidney disease, bone cancer, and nephrotoxicity (Shaki, 2019). Consumption of contaminated water in combination with higher rates of diabetes, birth defects, and liver disease found among Native populations may build upon other health issues (Indian Health Service, 2015), including impaired wound healing.

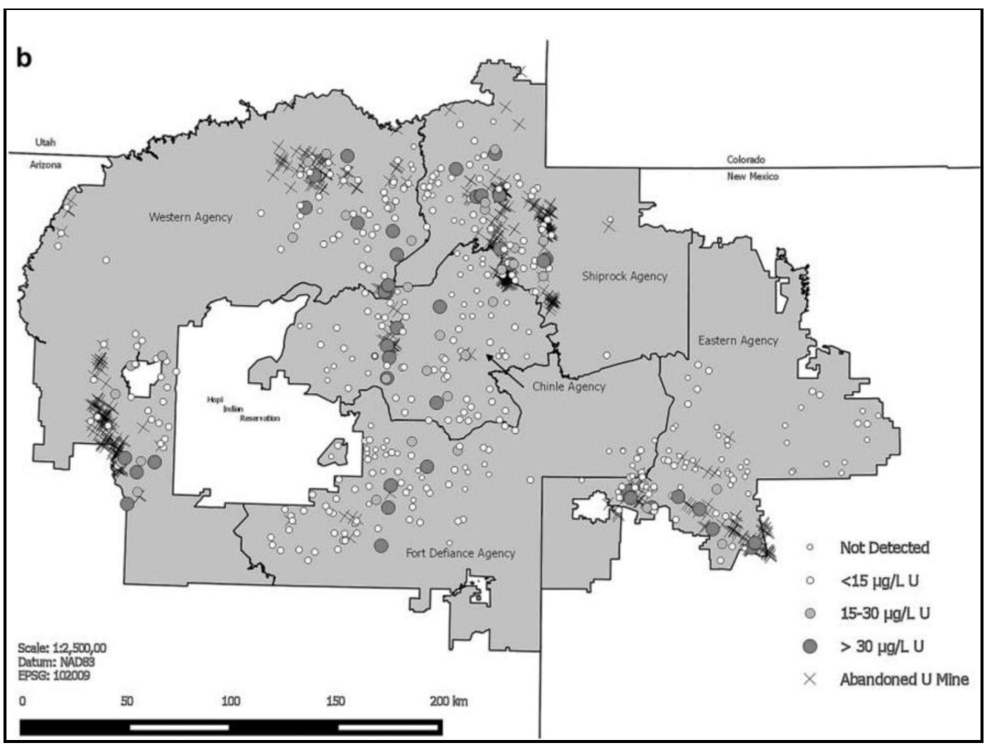

Figure 2. Map overview of the 464 unregulated water sources found in the Navajo nation. The 'X' symbol signifies a nearby abandoned uranium mine (Hoover, 2017).

1.3 Uranium Exposure and Health Effects

Exposure to DU can occur through internal or external pathways. External exposure primarily occurs through anti-armor weapons via fragments or debris (Shaki, 2019). Cite of exposure is usually small and affects the dermis (Bleise, 2003). Internal exposure can occur by three main pathways: ingesting DU-contaminated food or water, inhalation, and embedment through fragments or wounds contaminated with depleted uranium (Fischer, 2001). Internal uranium toxicity has been shown to increase the risk of lung cancer, kidney disease, and nephrotoxicity (Shaki, 2019). However, the prominent route of exposure remains through the consumption of U-contaminated drinking water (UNSCEAR, 2000). Once exposed, DU is absorbed and dispersed throughout the body. Depleted uranium has been shown to be held in tissue, organs, and bones. Furthermore, the bone acts as a reservoir for metals, including uranium. Following the end of the initial exposure, DU will continue to be released from the bone for months or even years (Zhu, 2009; Busby, 2010).

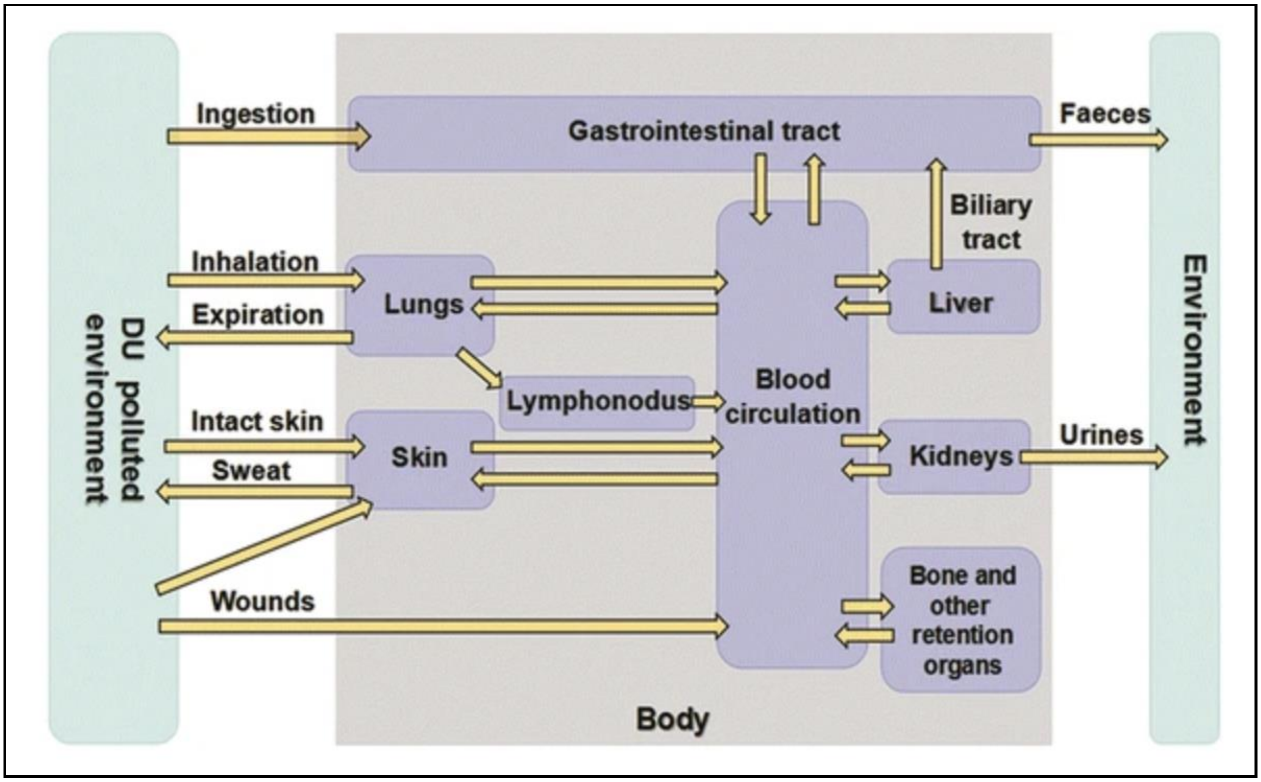

Figure 3. Biokinetics of depleted uranium. Following exposure, DU invades the circulatory system and is excreted via urine, excrement, sweat, and expiration, as well as tissue and other organs. Subsequently leading to the impairment of normal cellular functions. (Yue, 2018).

Chronic ingestion of DU results in alterations of the inflammation pathway, specifically in the immune cellular response (Dublineau, 2007). Similarly, another study found a dose-dependency between U and lymphocytes, as U induced oxidative stress due to increased ROS production, mitochondria membrane disruption, and cell death (Soltani, 2019). Acute high-dose exposure, whether it be ingested or inhaled, results in kidney failure, because of tubular necrosis (Kathren, 2008). Animal studies have shown single-dose U exposure as being nephrotoxic and sufficient in altering the biochemical framework of kidneys (Vicente-Vicente, 2010). Rats injected with uranyl acetate (a water-soluble uranium compound) were found to continually exhibit cortical scarring and interstitial nephritis following renal regeneration (Zimmerman, 2007). Chronic low-dose exposure in the drinking water of developing rats found altered responses in vocalization, reactivity, and arousal, as well as a decline in memory and brain mass (Briner, 2007). These *in-vivo* studies may serve as a possible indicator of the potentially harmful effects of long-term ingestion of U-contaminated drinking water.

Although several studies show that DU affects mitochondrial function, inflammatory responses, and immune cell content (Shaki, 2019), there is a lack of research surrounding heavy metal toxicity and the dermis (skin). Studies suggest that DU exposure to dermal fibroblast cells in a benchtop *in-vitro* cellular migration assay negatively affect wound closure and indicates a potentially toxic pathway for U in the form of contaminated wounds (Pinto, 2016). The hindering of wound healing mechanistic events from heavy metal toxicity has been shown to occur through decreased cell locomotion, metabolic activity (Cruz, 2021), and apoptotic death (Daraie, 2012) in fibroblast cells, demonstrating that exposure to DU has negative effects on the natural wound healing process through a variety of cytotoxic mechanisms. However, current literature is silent on descriptions of potential solutions or healing therapeutics to counteract this issue.

1.4 Electrospun Scaffolds

The extracellular matrix (ECM) consists mainly of collagen and elastin fibers alongside a network of glycoproteins and proteoglycans, which play a pivotal role in wound regeneration (Heath, 2010; Afsharian, 2021). The structure of ECM ranges from nanometer to micrometer in width and length, allowing its unique structure control over cell processes and attachment to nearby cells (Tracy, 2016; Zhu, 2019). Overall, the ECM provides cells with an array of key functions, including stability for cell anchoring, establishing orientation, formation of tissue microenvironment, and regulation over cell adhesion and migration (Ratner, 2004). Advances in the tissue engineering technique of electrospinning have allowed researchers to fabricate therapeutics that mirror the natural architecture of the ECM, resulting in heightened cell responses (Heath, 2010).

The technique of electrospinning can be found dating back to the 1930s (Formhals, 1934). One of the most influential wound-healing properties surrounding electrospinning is the ability to supply an ECM-like framework that can be broadly manipulated to fit an array of biomimetic and physicochemical applications (Afsharian, 2021; Asadi, 2023). Therapeutics, such as novel wound coverings, have been developed to promote the wound-healing process by adapting essential characteristics such as porosity, pore size, surface area, permeability, and structural integrity (Chen, 2017). These novel wound-healing devices are often applied to promote cellular migration, adhesion, and proliferation through various mechanisms, and may offer convenient delivery systems by incorporating a therapeutic agent into the wound-healing biomaterial (Afsharian, 2021).

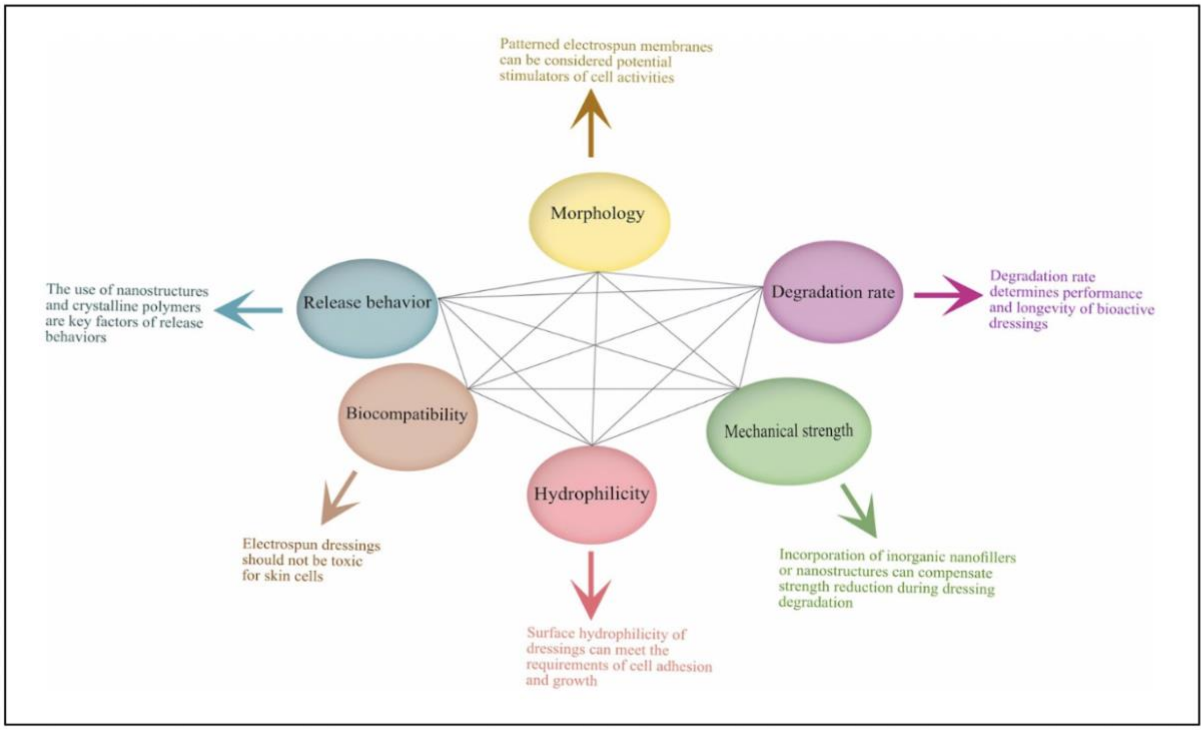

Figure 4. Network of scaffold characteristics. The illustration demonstrates what makes these novel wound-healing devices effective and highlights the interplay between parameters (Afsharian, 2021).

In recent studies, electrospun scaffolds have been used for biomimetic properties, probiotic delivery, antibacterial agents, skin regeneration, and nucleic acid carriers (Asadi, 2023; Afsharian, 2021). Furthermore, we propose that these novel electrospun wound healing scaffolds can be impregnated with unique chemical agents to facilitate delivery into the wound bed in an effort to neutralize or de-contaminate the tissue from DU exposure.

1.5 Rhamnolipids

Glycolipids are broadly studied biosurfactants containing a carbohydrate moiety attached to a long chain of aliphatic or hydroxy-aliphatic acid groups (Hogan, 2023). Of these glycolipids, rhamnolipids were initially isolated from the bacteria *Pseudomonas aeruginosa* and were characterized in 1949 by Jarvis and Johnson (Jarvis, 1949). In addition to being bio-derived, rhamnolipids are also produced synthetically through bio-inspired methods. Utilizing a synthetic route comes with advantages, including structure-specific production, purity, use of biorenewable materials, and especially metal recovery (Hogan, 2023).

Rhamnolipids primarily come in two forms, monorhamnolipid and dirhamnolipid (Ochoa-Loza, 2007). They have also displayed the ability to facilitate the removal of metals from the environment and other contaminated surfaces (Asselin, 2014). A study using rhamnolipids as a chelator found a concentration of 150 µM to be as effective as ethylenediaminetetraacetic acid (EDTA), a known chelating agent, in removing uranium from the soil surrounding mine sites (Asselin, 2014).

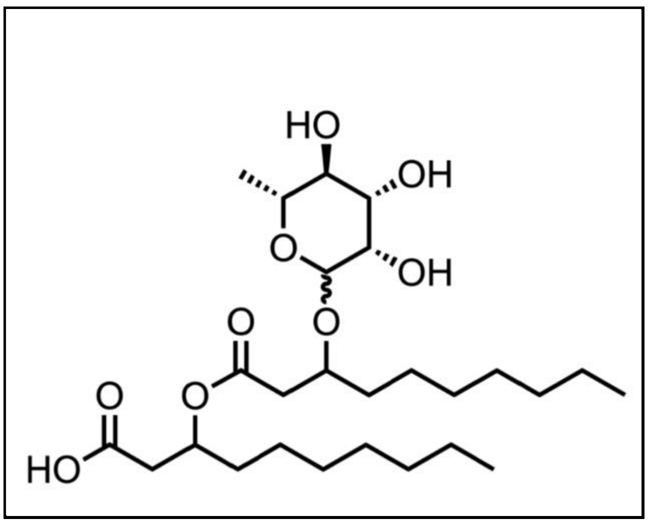

Figure 5. Chemical structure of mono-rhamnolipid (Rha-C10-C10) (adopted from GlycoSurf 2023). Rhamnolipids from GlycoSurf are bio-inspired surfactants produced by eco-friendly synthetic methods, and they are composed of hydrophilic and hydrophobic segments.

The mechanism of action between rhamnolipids and metals involves the carboxyl moiety binding with the metal. However, there is greater strength in the interaction between the metal and the hydroxyl groups on the rhamnose sugar moiety where a pocket is formed and the metal binds (Hogan, 2023). Furthermore, with a biosynthesized rhamnolipid, modifications to the structure could increase selectivity for various metals (Hogan, 2023).

1.6 Hypothesis

During initial "proof of concept" studies, an *in vitro* wound model was prepared using human dermal fibroblasts (hDFn) in combination with a synthetic rhamnolipid, a biodegradable surfactant with known environmental contaminant binding properties. It was hypothesized that utilizing rhamnolipids as a treatment for depleted uranium toxicity would result in favorable hDFn cell migration. Using the already established cellular migration assay, percent closure rates were measured after a synthetic wound was created and exposed to environmentally relevant levels of DU with and without our treatment, rhamnolipids. Recent studies have utilized electrospun scaffolds in various ways, including for antimicrobial agents, skin regeneration, probiotic delivery, and nucleic acid carriers (Afsharian, 2021). Furthermore, in this study, we proposed that these novel electrospun wound healing scaffolds could be impregnated with unique chemical agents, like rhamnolipids, to facilitate delivery into the wound bed in an effort to neutralize or de-contaminate the tissue from DU exposure. It was hypothesized that human dermal neonatal fibroblasts will exhibit normal cellular behavior and the ability to colonize electrospun scaffolds impregnated with rhamnolipids. In this study, scanning electron microscopy (SEM) was used to determine the visual presence of cells in scaffolds containing various concentrations of rhamnolipids compared with scaffolds without. Finally, when hDFn cells were cultured in the presence of the biosurfactant, rhamnolipid, hDFn cells would continue to exhibit favorable cellular processes. Using the viability assays PrestoBlue (metabolic activity) and CyQUANT Direct (living DNA content), the cellular response was measured and analyzed at their recommended concentrations for HDFn cells with and without treatment.

CHAPTER 2

Materials and Methods

2.1 Equipment and Software

Membrane integrity, cell metabolism, and DNA content were measured utilizing Gen5 software in tandem with the Biotek Instrument INC Synergy HT. Incubation temperature was set to 37℃.

2.2 Preparation of Depleted Uranium Solution

Approximately 0.005 g of uranyl nitrate (UN) crystals, purchased from American Scientific were weighed and solubilized in 40 mL of Dulbecco's modified eagle medium (DMEM) containing 10% fetal bovine serum (FBS) (DMEM complete) from Gibco to create an initial working stock solution. Uranyl nitrate stock underwent 60 seconds of pipette mixing to confirm proper disintegration prior to vacuum sterilization using a 0.22 μm filter. Molecular weight was used to calculate the appropriate starting molarity before utilizing weight-volume concentrations to obtain the following experimental dilutions: 0.1 μM, 0.2 μM, 1.0 μM, 2.0 μM, 10 μM, 20 μM made from the sterile-filtered stock solution.

2.3 Cell Culture of Neonatal Human Dermal Fibroblasts

Passage one Neonatal human dermal fibroblast (hDFn) cells were purchased from Cell Applications, Inc. (P1, lot #1734). The hDFn cells were incubated at 37℃, 5% CO_2, and passaged using a T-75 tissue culture flask from Corning, completing media changes every 48 hours until 90% confluency was met. Cells were subcultured at a density of 10 x 10^5 cells/mL, frozen in DMEM containing 10% DMSO, and stored at -80℃ for 24 hours before being placed in liquid nitrogen vapor phase for long-term preservation. The subsequent process was repeated until passage 4 isolates were frozen down.

2.4 Rhamnolipid Solution

About 0.0125g of rhamnolipids (Rha-C10-C10) from Glycosurf were weighed and diluted in 50 mL of 1x PBS to obtain a 200 μM rhamnolipid stock solution. The solution was heated prior to being vortexed for maximum dissolution and sterilized through a vacuum using a 0.22 μm filter. The molarity of rhamnolipid stock solution was found using actual mass (250 mg) and molecular weight to calculate experiment dilutions of 6.25 μM, 50 μM, and 100 μM.

2.5 Cellular Migration Assay

Human neonatal dermal fibroblasts (hDFn) passage 4, were seeded into a T-75 flask at 10 x 105 cells/mL density and grown in a standing incubator at 37℃, 5% CO_2. Once 90% confluence was reached, hDFn were subcultured into 12-well plates, and respective UN treatments with or without rhamnolipids were added. After 24 hours, contents were removed, and the monolayer of fibroblasts was scratched vertically using a sterile pipet tip creating the mock wound (Figure 6). Wells were then washed twice with HBSS. Respective treatments were added back into wells and cellular migration rates were monitored and imaged over time (0 hours, 12 hours, and 24 hours). Percent closure rates were collected using MATLAB.

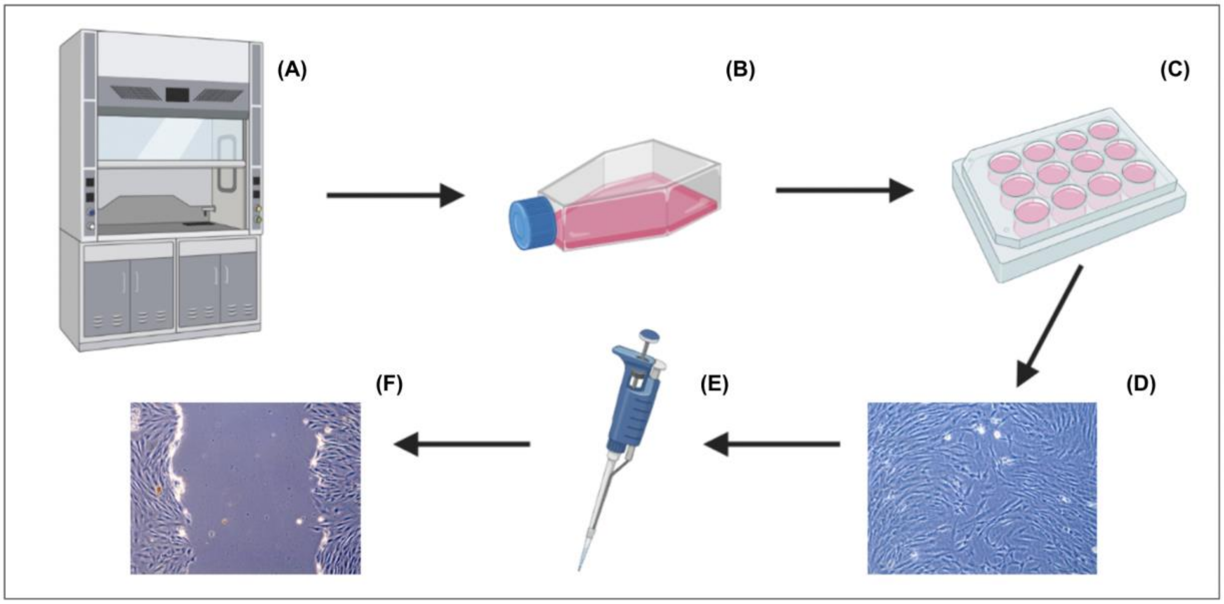

Figure 6. Visual depiction of the cellular migration assay process. Fibroblast cells were grown inside the BioSafety cabinet (A) in a T-75 flask (B) prior to subculturing into working 12-well plates (C). The monolayer of hDFn cells (D) was 'scratched' using a pipette tip (E) creating the mock wound (F) measured using MATLAB.

2.6 Construction of Electrospun Scaffolds

A protein polymer solution was prepared using a 10% bovine gelatin and Hexafluoroisopropanol (HFIP) solvent mixture in addition to varying concentrations of rhamnolipids (1%, 2.5%, 5%, and 10%). The protein polymer solution was charged at a high voltage (20KV) and a flow rate of 1mL/hour with a 12cm distance from the aluminum collector where fibers accumulated (Figure 7). Electrospun scaffolds were left to sit in a desiccator overnight prior to crosslinking for 1.5 hours with 50% glutaraldehyde vapors and placed overnight uncovered in the desiccator once again. Scaffolds were placed 4 inches beneath UV rays for sterilization for 1 hour on each side.

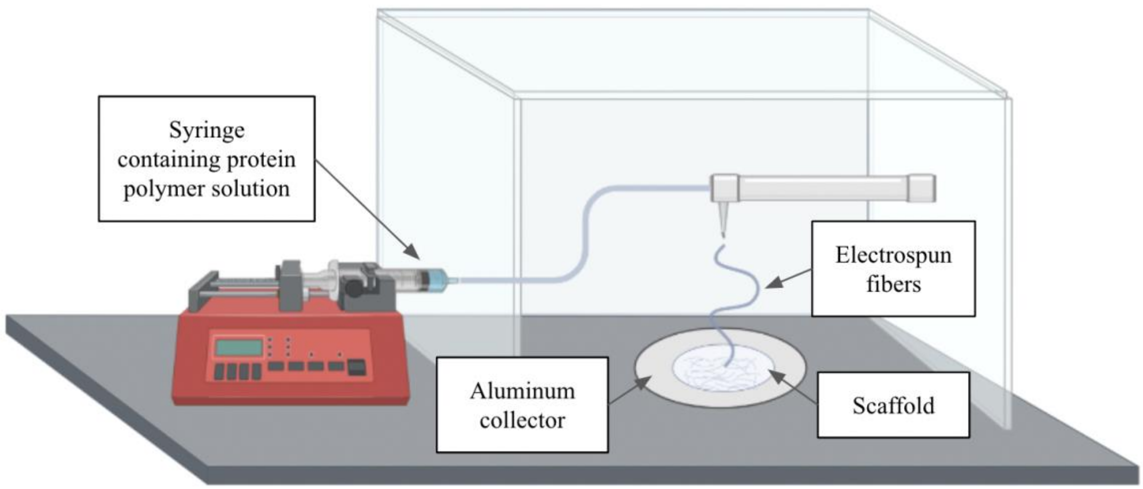

Figure 7. Visual representation of the general process of electrospinning. The polymer protein solution is charged with a high voltage from a positively charged needle onto a negatively charged aluminum collector where nanofibers are encouraged to form. The protein polymer solution consists of 10% bovine gelatin in an HFIP solvent mixture containing varying concentrations of rhamnolipids (1%, 2.5%, 5%, and 10%). The syringe was set at a flow rate of 1mL/hour with a distance of 12cm and 20KV.

2.7 Cellularization of Electrospun Scaffolds

Scaffold cellularization steps were completed aseptically inside the BioSafety cabinet in accordance with the laboratory's mammalian cell culture standard operating procedure. Biopsy punches of 10mm segments were removed from the control and treatment scaffolds (1%, 2.5%, 5%, and 10% rhamnolipid) and placed inside each well of a 48-well plate using sterile forceps that were treated in 70% ethanol for a minimum of 5 minutes. Approximately 1.5 ml of 1x PBS was used to rinse each membrane and then aspirated. Scaffolds sat in the biosafety cabinet for 1 hour to dry and adhere to the bottom of each well. Cells were then suspended onto scaffolds at a density of 11,000 cells/mL and allowed to rest for 30 minutes before placing into the standing incubator (37℃, 5% CO_2) for 48 hours.

2.8 Scanning Electron Microscopy

Scanning electron microscopy (SEM) was used to assess changes in nanofiber structure and cellular biocompatibility in impregnated scaffolds at various magnifications. Following cellularization, scaffolds were rinsed with 1x PBS and fixed with 2.5% glutaraldehyde (GA) in Na-cacodylate for 1 hour at room temperature. GA was aspirated and rinsed with approximately 0.5 mL of Na-cacodylate thrice for 15 minutes each. Thereafter, 0.5 mL of 2% Osmium in DI water was placed in wells and allowed to sit at room temperature for 1 hour and then rinsed three times for 5 minutes each with DI water only.

HDFn cells were dehydrated with approximately 0.5 mL of the following ethanol (EtOH) dilutions: 30%, 50%, 70%, and 95% EtOH for 10 minutes, and 100% EtOH for 10 minutes three times. While leaving 100% EtOH in wells, 0.5mL of hexamethyldisilazane (HMDS) was added (50:50 mixture) for 5 minutes. Contents were removed and 100% HMDS was placed in wells and left for 5 minutes twice. Samples were left in the fume hood to air dry for 1 hour. After mounting samples onto aluminum stubs and coating with gold palladium for 10 seconds, samples were viewed and imaged at various magnifications using the SEM, assessing for X, Y, and Z.

2.9 PrestoBlue and CyQUANT Direct Assay

PrestoBlue and CyQuant (PBCQ) direct confirmation assay (from ThermoFisher) for cell viability was used to assess the biocompatibility of hDFn cells in DMEM complete media with varying concentrations of rhamnolipids. Passage 5 hDFn cells were seeded at 11,200 cells/ml density into black wall, clear bottom 96-well tissue culture plates. The cells were placed inside the standing incubator at 37℃ and 5% CO_2 until reaching 70-90% confluence. Media was removed and replaced with the following rhamnolipid concentrations with an $n = 6$ for 24 hours: 6.25 µM, 50 µM, and 100 µM. The plate layout included blank wells containing DMEM complete media and the corresponding rhamnolipid concentrations. Following 24 hours, 100 µl was removed from each well and replaced with 10 µl of the PrestoBlue reagent. The plates were then incubated for 20 minutes at 37℃ and 5% CO_2 prior to being placed in the Biotek Synergy HT fluorescence microplate reader at 590 nm with a gain value of 35. Afterward, 100 µl of the CyQuant reagent composition was added to all wells and incubated for 60 minutes. The plates were read using the same microplate reader at 528 nm with a gain of 70. The relative fluorescence units (RFU) were produced for all wells, correlating with the metabolic output per unit of DNA.

2.11 Statistical Analysis

Statistically significant differences were determined using GraphPad Prism. The results of the cellular migration assay were analyzed with a one-way ANOVA and Tukey post hoc evaluation. The PBCQ assay was analyzed using a one-way ANOVA and Tukey post hoc evaluation. For all experiments, a p-value < 0.05 was considered statistically significant in this study.

CHAPTER 3

Results

3.1 Cellular Migration Assay

The cellular migration assay was used to determine if using rhamnolipids as a treatment for depleted-uranium toxicity would result in favorable hDFn cell migration, meaning the closure rate was not impaired or delayed in comparison to the control. After conducting the cellular migration assay, there was evidence to suggest that the migration rate, measured by percent closure, is increased in the presence of rhamnolipids, despite exposure to DU (Tukey's, $p<0.05$) (Figure 8).

HDFn cells exposed to 0.1 µM, 1.0 µM and 10 µM UN resulted in a significant increase in percent closure as early as 12 hours post-wound with the high concentration of rhamnolipids (50 µM) in comparison to the control (0.1µM + 50 µM: p-value = 0.021; 1.0 µM + 50 µM: p-value < 0.001; 10µM + 50 µM: p-value = 0.009). The cells exposed to 1.0 µM UN displayed a significant increase in percent closure 12 hours post-wound with the low concentrations of rhamnolipids (6.25 µM) (1.0 µM + 6.25 µM: p-value = 0.012). Throughout the experiment, 24 hours post-wound was considered closed as there was no significant difference in mean percent closure across the different treatments.

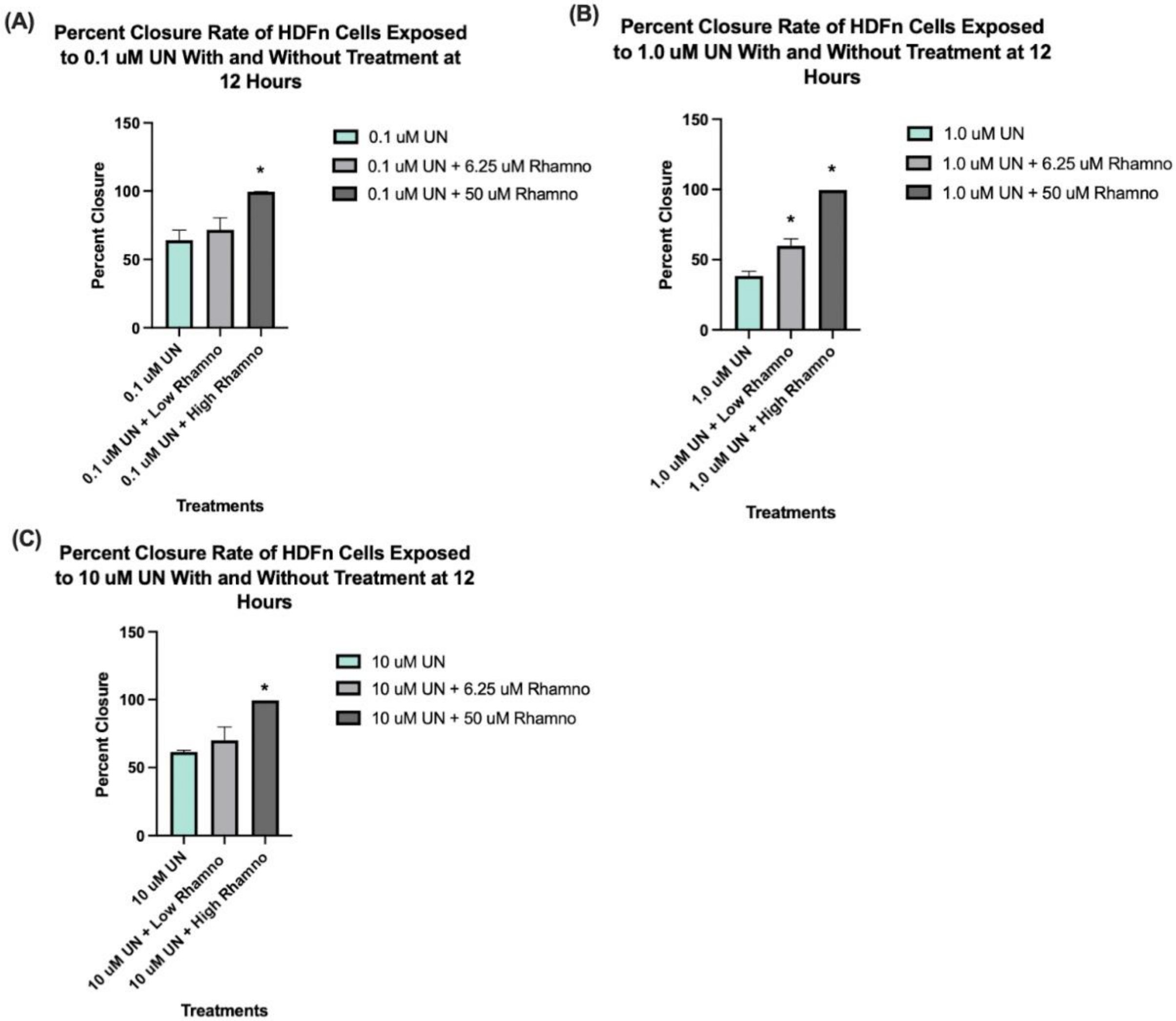

Figure 8. Analysis of percent closure rates of hDFn cells exposed to UN with and without treatment. Cells were exposed to varying concentrations of DU (0.1 µM (A), 1.0 µM (B), and 10 µM (C)) and treated with rhamnolipids (6.25 µM, and 50 µM) 24 hours before a mock wound was created using the bench top cell migration assay. Each bar graph illustrates average cell migration 12 hours post-wound +/- standard error of the mean (n = 3 for each treatment group, * = $p<0.05$).

Fibroblast cell migration was evaluated under conditions of a low and high concentration of rhamnolipids in the absence of UN ($F=32.81$, $p<0.001$) (Figure 9). There was a significant increase in cellular migration in wells treated with a high dose of rhamnolipids (Tukey's, $p = 0.001$). Furthermore, there was no significant difference in mean percent closure between the control and the low concentration of rhamnolipids.

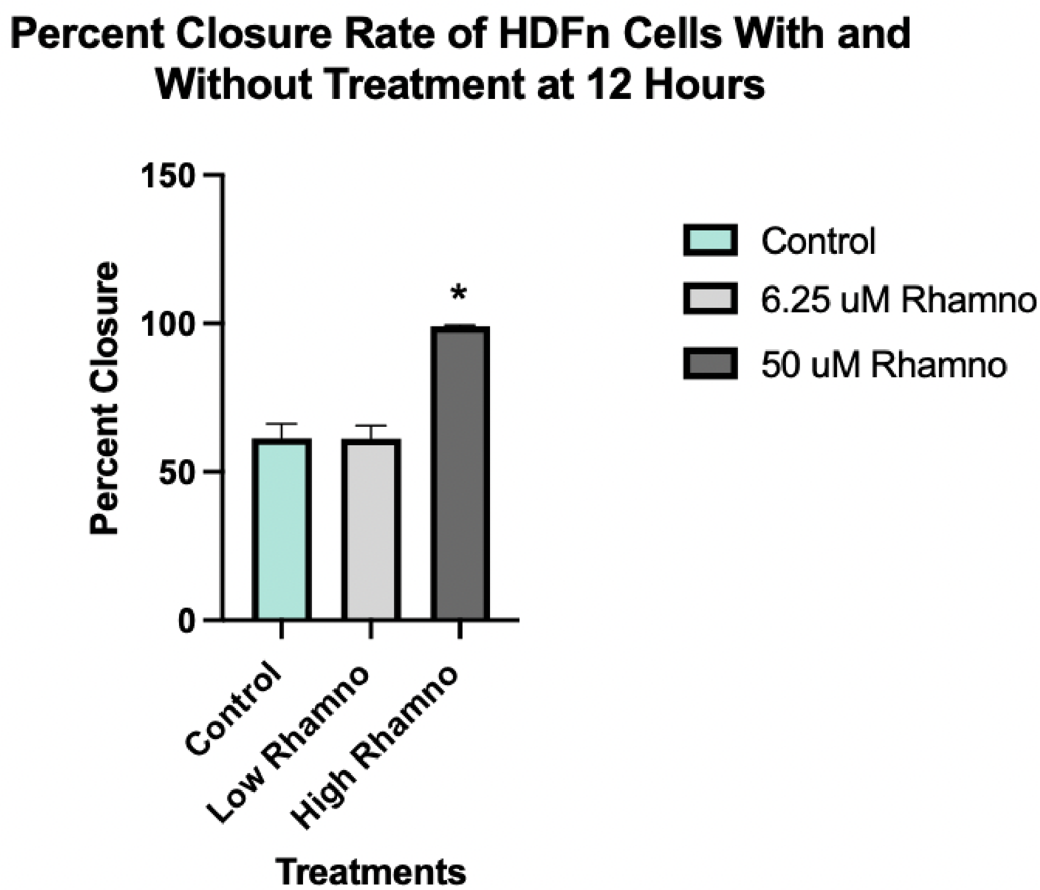

Figure 9. Analysis of percent closure rates of hDFn cells with and without treatment. Cells were treated with rhamnolipids (6.25 µM, and 50 µM) 24 hours before the creation of a mock wound. The bar graph illustrates average cell migration 12 hours post-wound +/- standard error of the mean ($n = 3$ for each treatment group, * = $p < 0.05$).

3.2 Scanning Electron Microscopy

SEM images were used to visually determine if the hDFn cells were able to demonstrate normal cellular behavior (elongation of filipodia, ability to adhere onto structure) on scaffolds impregnated with rhamnolipids compared to the control with no rhamnolipids. The bare control and treatment scaffolds, containing no cells, were mounted onto aluminum stubs, and coated with gold palladium for 10 seconds. Cellularized scaffolds (both control and treatment) were seeded with hDFn cells and fixed using glutaraldehyde, dehydrated with hexamethyldisilane, air-dried for 1 hour, sputter coated with gold palladium, and mounted with carbon tape. On the SEM, the SE2 and InLens detectors were used, as well as an accelerating voltage of 2.00 kV – 5.00 kV with magnifications ranging from 300 X and 999 X.

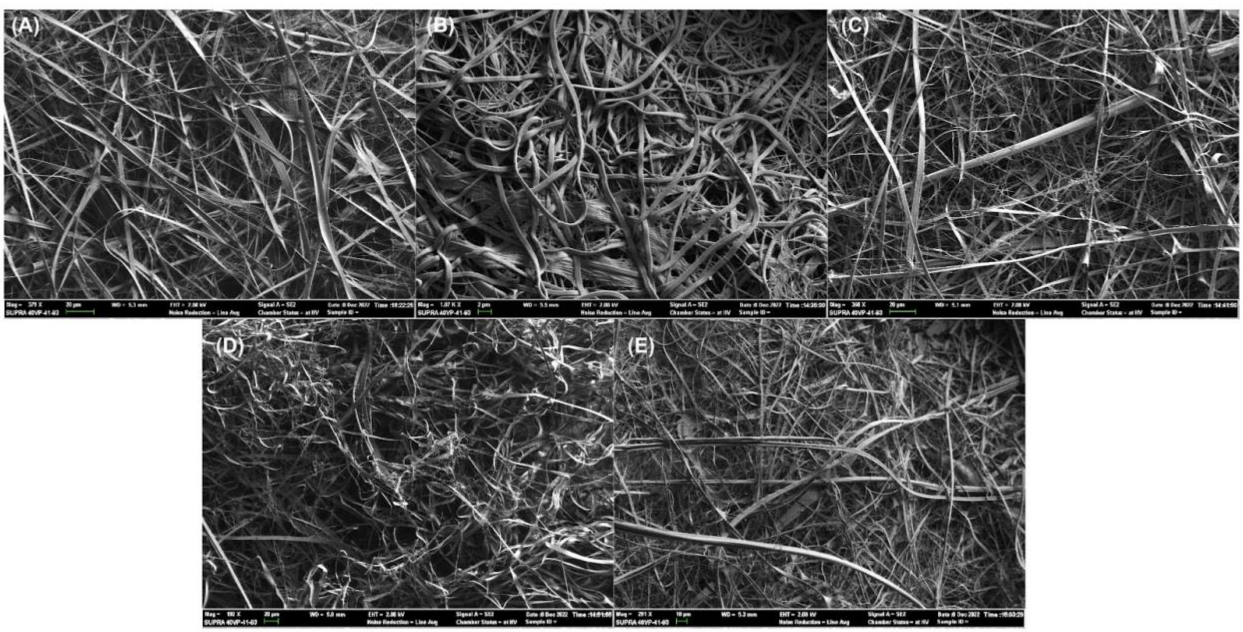

Figure 10. SEM images of bare (no cells) electrospun scaffolds. Image A corresponds with a control (containing no treatment) scaffold meanwhile B-E corresponds to varying concentrations (1%, 2.5%, 5%, and 10%) of rhamnolipids. SEM images of impregnated scaffolds displayed a similar porosity throughout the experiment despite an increase in rhamnolipid concentrations.

The control scaffold, image A from Figure 10, was not impregnated with rhamnolipids or had hDFn cells seeded onto it. In particular, the observable porosity is not structurally different in this image compared to the other images depicting impregnated scaffolds without cells. As the percentage of rhamnolipids increased, the porosity of the scaffold remained relatively similar to the control. Furthermore, hDFn cells were able to grow and migrate onto all the treatment scaffolds (Figure 11) at 1%, 2.5%, 5%, and 10%. Visually, the hDFn cells appeared to have been able to adhere and colonize onto impregnated scaffolds which could be further explored to better understand the cytocompatibility of rhamnolipids and if their morphology is influenced by the concentration of the surfactant.

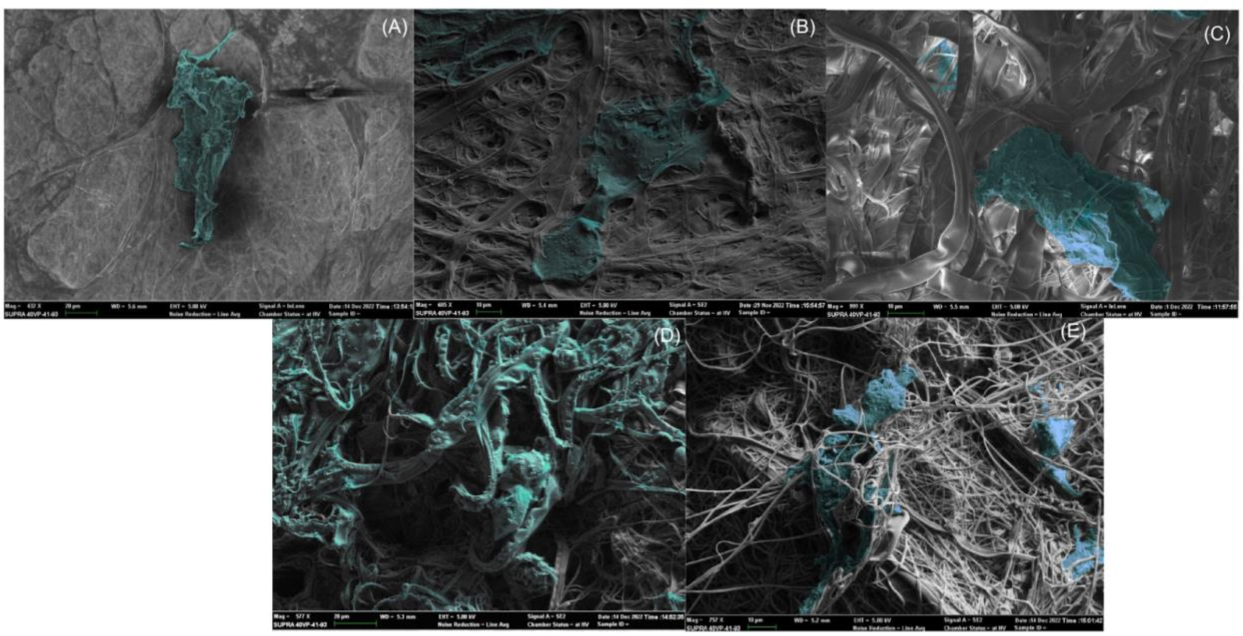

Figure 11. SEM images of electrospun cellularized scaffolds. HDFn cells are highlighted in blue. Image A corresponds to a cellularized control scaffold, meanwhile, B-E corresponds to varying concentrations (1%, 2.5%, 5%, and 10%) of rhamnolipids with hDFn cells. Impregnated scaffolds were shown capable of growing hDFn cells into their structure.

3.3 PrestoBlue and CyQUANT Direct Assay

The PrestoBlue and CyQUANT Direct assays were used to determine the cellular compatibility of hDFn cells when in the presence of rhamnolipids. The PrestoBlue assay is a resazurin-based solution when upon entering a living cell, the reagent is reduced to resorufin which is red in color and fluorescent. The overall health of the cell can be observed by changes in fluorescence and subsequently absorbance. Metabolically active cells constantly convert the PrestoBlue reagent whereas non-viable cells cannot reduce the dye and do not produce a change in signal. The CyQUANT Direct assay is a cell-permeant green nucleic acid stain that is combined with a masking dye reagent. The masking dye stops the staining of non-viable cells or cells with compromised cell membranes, resulting in only the viable cells being stained. The CyQUANT Direct assay measures proliferation as well as membrane integrity. The data was evaluated using GraphPad Prism to run a one-way ANOVA.

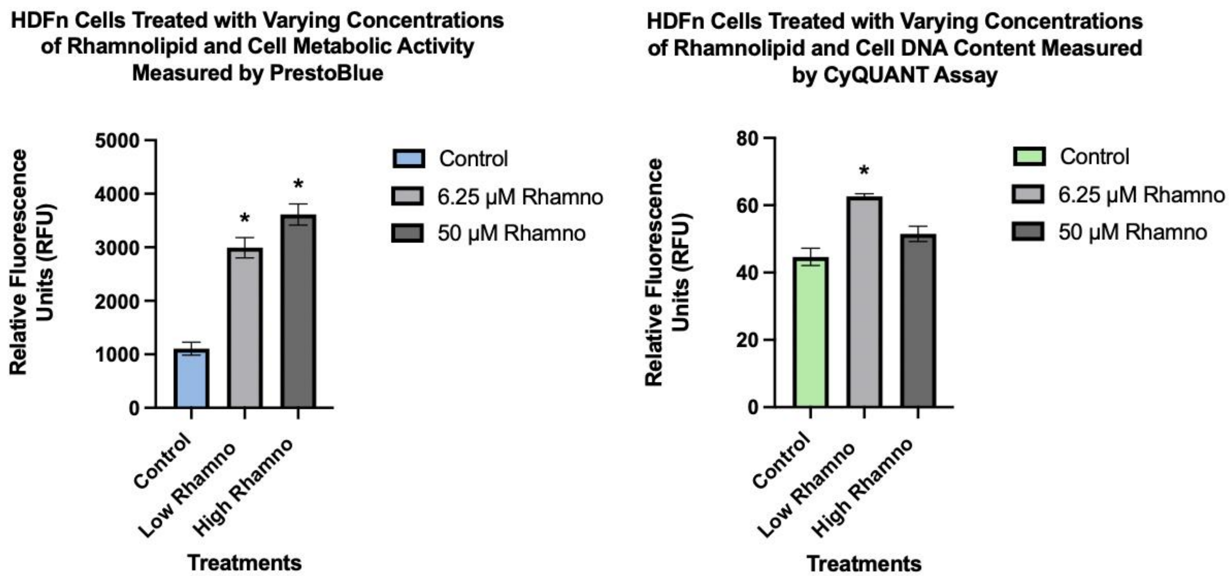

Figure 12. Analysis of metabolic activity (left graph) and DNA content (right graph) of hDFn cells with and without rhamnolipids. The bar graphs show the average RFU values +/- standard error of the mean (n = 6 for each treatment group, * = p < 0.05).

The results of the PrestoBlue (left graph) assay demonstrated a significant increase in metabolic activity from percent concentrations of 6.25 µM (Tukey's, p<0.001), and 50 µM (Tukey's, p<0.001) compared to the control (Figure 12). A one-way ANOVA of the PrestoBlue assay resulted in a P-value <0.001 and an F-value of 57.16. The CyQUANT Direct assay (right graph) results demonstrated a significant increase in cellular DNA content with the low concentration of rhamnolipids (Tukey's, p<0.001). A one-way ANOVA of the CyQUANT Direct assay resulted in a P-value <0.001 and an F-value of 20.00. Meanwhile, there was no significant difference between the living DNA content of the high concentration of rhamnolipids compared to the control.

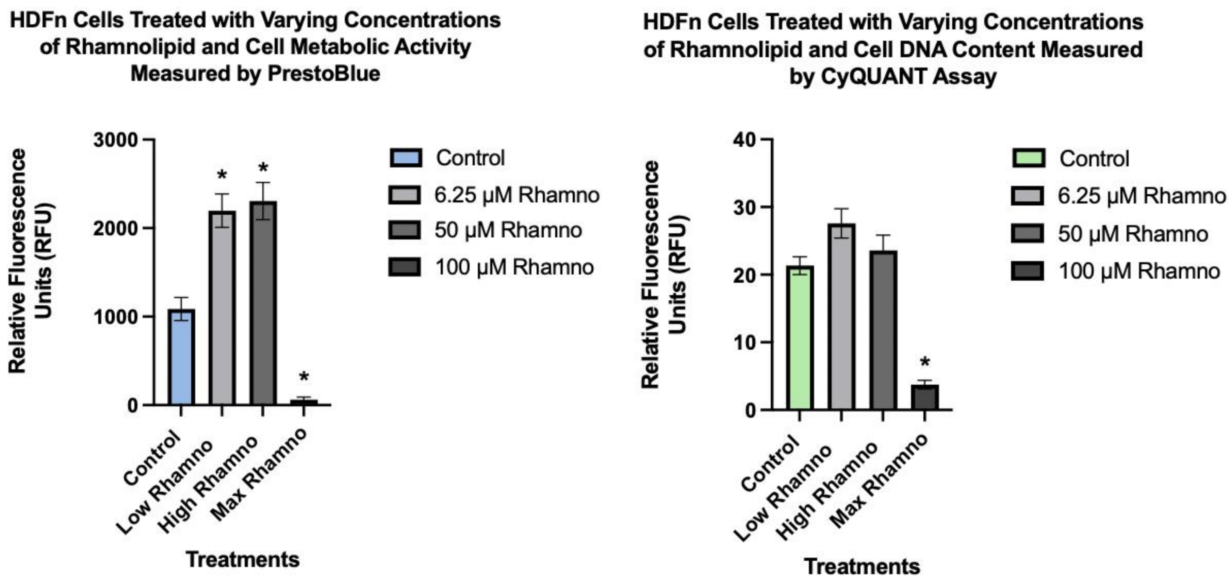

Figure 13. Analysis of metabolic activity (left graph) and DNA content (right graph) of hDFn cells with and without varying concentrations of rhamnolipids. The bar graphs show the average RFU values +/- standard error of the mean (n = 12 for each treatment group, * = p < 0.05).

The results of the PrestoBlue (left graph) assay suggested a significant increase in metabolic activity from percent concentrations of 6.25 µM (Tukey's, $p<0.001$), and 50 µM (Tukey's, $p<0.001$) compared to the control (Figure 12). A one-way ANOVA of the PrestoBlue resulted in a P-value <0.001 and an F-value of 45.85. Meanwhile, there was a significant decrease in metabolic activity with the maximum concentration of rhamnolipids (100 µM) in comparison to the control (Figure 13). The CyQUANT Direct assay (right graph) demonstrated a significant decrease in cellular DNA content with the 100 µM concentration of rhamnolipids as compared to the control. A one-way ANOVA of the CyQUANT Direct assay resulted in a P-value <0.001 and an F-value of 37.04. Furthermore, there was no significant difference between the living DNA content of the low and high concentrations of rhamnolipids in comparison to the control. The max concentration of rhamnolipids could provide a threshold for usable dosages of our treatment in future studies.

CHAPTER 4

Discussion

Internal uranium toxicity through the consumption of contaminated water is among the more prominent routes of heavy metal exposure and has been shown to increase the risk of various diseases and cancers (Shaki, 2019; UNSCEAR, 2000). Previous reports indicate that depleted uranium exposure to dermal fibroblast cells in a benchtop *in-vitro* cellular migration model adversely affected wound closure, and indicated a potentially toxic pathway for DU in the form of contaminated wounds (Pinto, 2016). Furthermore, studies have shown that exposure to U also had adverse physiological and mechanistic effects on hDFn cells, and subsequently the wound healing process (Cruz, 2021). However, current methods lack potential solutions or wound-healing devices to remedy this issue. The current study is among the first to evaluate rhamnolipids, a biodegradable surfactant with metal binding properties, in an *in vitro* wound model using hDFn (skin) cells. It was hypothesized that utilizing rhamnolipids as a treatment for depleted uranium toxicity would result in favorable hDFn cell migration. The results of this assay revealed that with the high concentration of rhamnolipids, the hDFn cells were able to reach complete closure within 12 hours– despite exposure to DU.

The tissue engineering technique of electrospinning was implemented in research as early as the 1930s (Formhals, 1934). Since then, plenty of studies have utilized scaffolds for an array of different functions. Novel electrospun therapeutics came about to promote the wound-healing process by mimicking the natural extracellular matrix and its characteristics to promote cell migration, adhesion, and proliferation (Afsharian, 2021). However, incorporating rhamnolipids into these three-dimensional wound healing devices could serve as an effective agent in neutralizing uranium toxicity. Furthermore, it was hypothesized that hDFn cells would continue to exhibit normal cellular behavior and the ability to colonize those electrospun scaffolds impregnated with rhamnolipids. In the current study, these novel wound healing devices were able to be incorporated with unique chemical agents to facilitate delivery into the wound bed to de-contaminate the tissue from depleted uranium exposure. Through the use of scanning electron microscopy (SEM), the presence of hDFn cells in scaffolds containing various concentrations of rhamnolipids and scaffolds without was visually confirmed.

Rhamnolipids are broadly studied biosurfactants that were primarily isolated from the pathogen *Pseudomonas aeruginosa* (Banat, 2010). In addition to being bio-derived, rhamnolipids can also be produced synthetically. Synthetic production has numerous advantages, including structure-specific production, purity, use of biorenewable materials, and heavy metal recovery (Hogan, 2023). The advantages of utilizing biosurfactants in this study include compatibility with human skin and low irritancy (Maier, 2000). Reports found rhamnolipids to increase oxygen saturation on the surface of wounds through their effect as a surfactant. This effect helps support the migration of cells involved in the natural wound-healing process and promotes antibacterial properties (Bharali, 2013; Rodrigues, 2006). Based on these findings, it was hypothesized that when hDFn cells were cultured in the presence of the biosurfactant, rhamnolipid, hDFn cells would continue to exhibit favorable cellular processes. Using viability assays to measure metabolic activity and the living DNA content of the hDFn cells, the cellular response was measured and analyzed at their recommended concentrations with and without treatment. The data demonstrated a significant increase in metabolic activity in cells following 24 hours of exposure. Meanwhile, there were no significant differences in living cell DNA after 24 hours of exposure to rhamnolipids.

The current study focused on using rhamnolipid's metal-binding ability to sequester wounds contaminated with depleted uranium. It was then hypothesized that utilizing rhamnolipids as a treatment for depleted uranium toxicity would result in favorable hDFn cell migration. The hypothesis was supported through the cellular migration assay. As seen in Figure 8, the results of the assay at 12 hours demonstrated a significant increase in the percent closure rate (p-value < 0.05) of cells with the high concentration of rhamnolipids (50 uM) regardless of the presence of DU at all concentrations (0.1 uM, 1.0 uM, 10 uM). We can conclude from this data that rhamnolipids were able to neutralize the harmful effects of DU and allow cells to close at a higher rate despite exposure to heavy metals. Similarly, in Figure 9, there is a trend shown with cells and the 50uM of rhamnolipids. After 12 hours, the hDFn cells were found to have had an increase in percent closure (p-value < 0.05), suggesting that outside of acting as a chelator, rhamnolipids surfactant abilities were able to excite the hDFn cells' ability to migrate toward each other.

This study is among the first to describe the effects of rhamnolipids as a treatment against acute *in vitro* DU exposure to hDFn cells in wound healing. However, other methods have described increased wound healing *in vivo* by applying di-rhamnolipids onto burn wounds on Swiss–Webster mice to measure if there was an increase in wound healing. The results from the study found that the wound closure rate measured on days 14, 21, and 28 was significantly faster in mice that were administered the 0.1% di-rhamnolipid ointment than not (Stipcevic, 2006). Moreover, these findings suggest that those who experience a delay in wound healing following exposure to DU may utilize rhamnolipids in assisting fibroblast migration and helping improve wound healing.

In addition, this research investigated whether these novel wound healing devices were able to be incorporated with unique chemical agents to facilitate delivery into the wound bed to de-contaminate the tissue from depleted uranium exposure. As seen in Figure 10, scaffolds were able to undergo the high voltage of the electrospinner with all concentrations of our treatment (1%, 2.5%, 5%, and 10%). The resulting SEM images supported this prediction and gave a sufficient indication of the visual presence of rhamnolipids in the scaffolds as there is a slight variation in thickness as percentages increase, with no overall visual change in structure. Subsequently, it was hypothesized that hDFn cells would continue to exhibit normal cellular behavior and the ability to colonize those electrospun scaffolds impregnated with rhamnolipids. The visual behavior of the cells can be seen showing indications of normal cell behavior, as fibroblasts are able to elongate along the scaffold structure at all concentrations of the treatment. As seen in Figure 11, hDFn cells were able to colonize and adhere to impregnated scaffolds, indicating signs of a favorable environment. Therefore, the hypothesis was supported through quantitative analysis. Additionally, these results are consistent with prior literature where scaffolds were impregnated with rhamnolipids to better serve in the drug delivery of usnic acid, which documented a strong antibacterial, and biocompatible treatment of bone regeneration and osteomyelitis (Falakaflaki, 2022).

The biocompatibility of rhamnolipids and hDFn cells was also assessed. Acute 24-hour exposure of skin cells to various concentrations of rhamnolipids was evaluated. It was hypothesized that when hDFn cells were cultured in the presence of the biosurfactant, rhamnolipid, hDFn cells would continue to exhibit favorable cellular processes. This hypothesis was supported by the PrestoBlue and CyQUANT Direct assays to determine the cellular compatibility of hDFn cells when in the presence of rhamnolipids. The PrestoBlue assay is a resazurin-based solution where the reagent is red in color and fluorescent. The overall metabolic activity of the cell can be observed by changes in fluorescence and absorbance. The CyQUANT Direct assay measures living DNA content and is a cell-permeant green nucleic acid stain that is combined with a masking dye reagent that hinders the staining of non-viable cells or cells with compromised cell membranes, resulting in only the viable cells being stained. As shown in Figure 12, a one-way ANOVA test was used to statistically analyze the results of the PBCQ data followed by Tukey's post hoc test.

The one-way ANOVA for the PrestoBlue produced a p-value < 0.001, meaning we reject the null in favor of the alternative indicating that there is a difference in means. Moreover, the post hoc Tukey's test supports this claim as both the low and high concentrations were found to have a significant increase in metabolic activity in comparison to the control with a p-value < 0.001 for each. There is a similar trend seen in Figure 13, where again the one-way ANOVA of the PrestoBlue resulted in a P-value <0.001 and the low and high concentrations were found to have a significant increase in metabolic activity in comparison to the control with a p-value < 0.001. The importance of these findings indicates rhamnolipids outside of their ability to bind to heavy metals, are able to stimulate an increase in hDFn cell activity. Since hDFn cells are vital in the proliferation stage of wound healing, future studies could investigate rhamnolipids to aid in accelerating the wound healing process. However, the max concentration of our treatment (100 uM) resulted in a significant decrease in metabolic activity with a p-value < 0.001. Decreased metabolism with the max concentration is significant for a couple of reasons. First, these results help define a threshold of usable dosages for rhamnolipids in future studies. Additionally, too high of rhamnolipids could have punctured the cell membranes, as the surfactant is a surface-active agent (Hogan, 2023).

The one-way ANOVA for the CyQUAT direct assay showed a p-value < 0.001, which means the null hypothesis was rejected in favor of the alternative. Tukey's post hoc test supports this claim as the low concentration of rhamnolipids was found to have a significant increase in DNA content in comparison to the control with a p-value < 0.001. Indicating that the rhamnolipids promoted an increase in living cells in its presence. In addition, Figure 13 showed the one-way ANOVA of the CyQUAT direct assay resulted in a P-value <0.001. However, there was no significant difference between the living DNA content of the low and high concentrations of rhamnolipids in comparison to the control as seen with Tukey's test. The importance of no significant increase or decrease in DNA content between the low and high treatments to the control indicates that there were no comparable differences in living DNA in cells with and without treatment present. Furthermore, the max concentration of rhamnolipids demonstrated a significant decrease in living DNA content with a p-value < 0.001. A decrease in DNA content of hDFn cells with the max concentration is notable as the data helps define a firm threshold of usable concentrations of rhamnolipids in future studies. This data was also consistent with previously published studies that describe enhanced metabolic activity in bacteria when inoculated with rhamnolipids and showed an increase in bacterial growth for the purpose of improving the remediation of contaminated soil (Tahseen, 2016).

In summary, the current study demonstrated that treating DU-exposed hDFn cells with rhamnolipids by utilizing the established cellular migration assay, demonstrated a surge in cellular migration and proliferation despite the presence of the heavy metal. SEM images illustrated the cytocompatibility between rhamnolipid-impregnated scaffolds and hDFn cells through their ability to grow and migrate into the structure at all concentrations of our treatment. The cellular biocompatibility of rhamnolipids was measured using the PBCQ assay where low and high concentrations of our treatment led to an increase in cell metabolism and showed no significant decrease in viability aside from our max dosage which may serve as a threshold for future studies. These findings are among the first to explore the effects of rhamnolipids as a treatment against internal DU exposure by using electrospun scaffolds alongside hDFn cells during the proliferation stage of wound healing to provide a healing therapeutic to treat those individuals affected by chronic exposure to U-contaminated water throughout the American Southwest.

REFERENCES

Afsharian, Y. P., & Rahimnejad, M. (2021). Bioactive electrospun scaffolds for wound healing applications: A comprehensive review. *Polymer Testing*, *93*, 106952. https://doi.org/10.1016/J.POLYMERTESTING.2020.106952

Asadi, N., Del Bakhshayesh, A.R., Sadeghzadeh, H. et al. Nanocomposite Electrospun Scaffold Based on Polyurethane/Polycaprolactone Incorporating Gold Nanoparticles and Soybean Oil for Tissue Engineering Applications. J Bionic Eng (2023). https://doi.org/10.1007/s42235-023-00345-x

Asselin, S., Ingram, J.C., "Uranium Leaching from Contaminated Soil Utilizing Rhamnolipid, EDTA, and Citric Acid", Applied and Environmental Soil Science, vol. 2014, Article ID 462514, 6 pages, 2014. https://doi.org/10.1155/2014/462514

Banat, I. M., Franzetti, A., Gandolfi, I., Bestetti, G., Martinotti, M. G., Fracchia, L., Smyth, T. J., & Marchant, R. (2010). Microbial biosurfactants production, applications, and future potential. In Applied Microbiology and Biotechnology (Vol. 87, Issue 2). https://doi.org/10.1007/s00253-010-2589-0

Bharali P., Saikia J.P., Paul S., Konwar B.K. Colloidal silver nanoparticles/rhamnolipid (SNPRL) composite as novel chemotactic antibacterial agent. Int J Biol Macromol, 61 (2013), pp. 238-242, 10.1016/j.ijbiomac.2013.07.006

Bleise A., Danesi P., Burkart W. Properties, use and health effects of depleted uranium (DU): A general overview J. Environ. Radioact. 2003; 64: 93 -112

Briner, Wayne. “The toxicity of depleted uranium.” *International journal of environmental research and public health* vol. 7,1 (2010): 303-13. doi:10.3390/ijerph7010303

Briner W. Neurotoxicology of depleted uranium in adult and developing rodents. In: Miller A, editor. Depleted Uranium, Properties, Uses, and Health Consequences. CRC Press; New York, NY, USA: 2007. pp. 67–74.

Bronson I. Pinto, Aaron J. Tabor, Diane M. Stearns, Robert B. Diller, and Robert S. Kellar. A Bench-Top In Vitro Wound Assay to Demonstrate the Effects of Platelet-Rich Plasma and Depleted Uranium on Dermal Fibroblast Migration. Applied In Vitro Toxicology. Sep 2016.151-156.http://doi.org/10.1089/aivt.2016.0001

Brugge, Doug, and Rob Goble. “The history of uranium mining and the Navajo people.” *American journal of public health* vol. 92,9 (2002): 1410-9. doi:10.2105/ajph.92.9.1410

Busby C. The health effects of exposure to uranium and uranium weapons ECRR 2010; 2 : 1 -29

Chen, S., Liu, B., Carlson, M. A., Gombart, A. F., Reilly, D. A., & Xie, J. (2017). Recent advances in electrospun nanofibers for wound healing. In *Nanomedicine* (Vol. 12, Issue 11). https://doi.org/10.2217/nnm-2017-0017

Dublineau I., Grandcolas L., Grison S., Baudelin C., Paquet F., Voisin P., Aigueperse J., Gourmelon P. Modifications of inflammatory pathways in rat intestine following chronic ingestion of depleted uranium Toxicol. Sci. 2007; 98 : 458 -68

EPA. Us Epa (2023). https://www.epa.gov/radiation/radionuclide-basics-uranium

EPA. Us Epa (2023). https://www.epa.gov/navajo-nation-uranium-cleanup/abandoned-mines-cleanup

Erikson, R. L., Hostetler, C. J., Divine, J. R., & Price, K. R. *A review of the environmental behavior of uranium derived from depleted uranium alloy penetrators*. United States (1990): https://doi.org/10.2172/5105913

Falakaflaki, M., Varshosaz, J., & Mirian, M. (2022). Local delivery of usnic acid loaded Rhamnolipid vesicles by gelatin / tragacanth gum / montmorillonite/ vanillin cryogel scaffold for expression of osteogenic biomarkers and antimicrobial activity. *Journal of Drug Delivery Science and Technology*, *69*. https://doi.org/10.1016/j.jddst.2022.103147

Fischer H. Depleted uranium: sources, exposure and health effects World Health Organ. 2001; 4 : 324 -5

Formhals, A. Process and apparatus for preparing artificial threads. US Patent No. 1,975,504, 1934.

Hogan, D. E., Boxley, C. J., Stolley, R. M., & Maier, R. M. (2023). Bioinspired glycolipids: Metals interactions and aqueous-source metal recovery technologies. *Biosurfactants*, 47–67. https://doi.org/10.1016/B978-0-323-91697-4.00003-X

IAEA. Depleted Uranium (2023). https://www.iaea.org/topics/spent-fuel-management/depleted-uranium

Jarvis, F. G., & Johnson, M. J. (1949). A Glyco-lipide Produced by Pseudomonas Aeruginosa. *Journal of the American Chemical Society*, *71*(12). https://doi.org/10.1021/ja01180a073

Kathren, R.L., Burklin R.K. Acute chemical toxicity of uranium. Health Phys. 2008;94:170–179.

Keith S., Faroon O., Roney N., et al. Toxicological Profile for Uranium. Atlanta (GA): Agency for Toxic Substances and Disease Registry (US); 2013 Feb. 3, HEALTH EFFECTS. Available from: https://www.ncbi.nlm.nih.gov/books/NBK158798/

Maier, R.M., Soberon-Chavez G. Pseudomonas aeruginosa rhamnolipids: biosynthesis and potential applications. *Appl Microbiol Biot.* 2000; 54: 625-633

Ochoa-Loza, F. J., Noordman, W. H., Jannsen, D. B., Brusseau,M. L., and Maier, R. M., “Effect of clays, metal oxides, and organic matter on rhamnolipid biosurfactant sorption by soil,” Chemosphere, vol. 66, no. 9, pp. 1634–1642, 2007.

Rani, Asha, and Surinder Singh. “Analysis of Uranium in Drinking Water Samples Using Laser Induced Fluorimetry.” *Health Physics*, vol. 91, no. 2, Aug. 2006, pp. 101–07, doi:10.1097/01.HP.0000202233.64500.89.

Ringholtz R.C. *Uranium Frenzy: Boom and Bust on the Colorado Plateau.* New York, NY: WW Norton & Co; 1989.

Rodrigues L., Banat I.M., Teixeira J., Oliveira R. Biosurfactants: potential applications in medicine. J Antimicrob Chemother, 57 (2006), pp. 609-618, 10.1093/jac/dkl024

Soltani M., Zarei M.H., Salimi A., Pourahmad J. Mitochondrial protective and antioxidant agents protect toxicity induced by depleted uranium in isolated human lymphocytes J. Environ. Radioact. 2019; 203: 112 -6

Stipcevic, T., Piljac, A., & Piljac, G. (2006). Enhanced healing of full-thickness burn wounds using di-rhamnolipid. *Burns*, 32(1). https://doi.org/10.1016/j.burns.2005.07.004

Tahseen, R., Afzal, M., Iqbal, S., Shabir, G., Khan, Q. M., Khalid, Z. M., & Banat, I. M. (2016). Rhamnolipids and nutrients boost remediation of crude oil-contaminated soil by enhancing bacterial colonization and metabolic activities. *International Biodeterioration and Biodegradation*, *115*. https://doi.org/10.1016/j.ibiod.2016.08.010

Tracy, L. E., Minasian, R. A., & Caterson, E. J. (2016). Extracellular Matrix and Dermal Fibroblast Function in the Healing Wound. In *Advances in Wound Care* (Vol. 5, Issue 3). https://doi.org/10.1089/wound.2014.0561

UNSCEAR S. Effects of Ionizing Radiation: 2000 Report to the General Assembly, with Scientific Annexes, Volume 2: Effects 2000.

Vicente-Vicente L, Quiros Y, Perez-Barriocanal F, Lopez-Novoa JM, Lopez-Hernandez FJ, Morales AI. Nephrotoxicity of uranium: pathophysiological, diagnostic and therapeutic perspectives. Toxicol Sci. 2010;118:324–47.

Yue, Y.C., Li, M.H., Wang, H.B. et al. The toxicological mechanisms and detoxification of depleted uranium exposure. Environ Health Prev Med 23, 18 (2018). https://doi.org/10.1186/s12199-018-0706-3

Zhu G., Tan M., Li Y., Xiang X., Hu H., Zhao S. Accumulation and distribution of uranium in rats after implantation with depleted uranium fragments J. Radiat. Res. 2009; 50: 183 -92 [PubMed]

Zhu, M., Li, W., Dong, X., Yuan, X., Midgley, A. C., Chang, H., Wang, Y., Wang, H., Wang, K., Ma, P. X., Wang, H., & Kong, D. (2019). In vivo engineered extracellular matrix scaffolds with instructive niches for oriented tissue regeneration. *Nature Communications*, *10*(1). https://doi.org/10.1038/s41467-019-12545-3